

Atomistic simulations of the size, orientation, and temperature dependence of tensile behavior in GaN nanowires

Zhiguo Wang,^{1,*} Xiaotao Zu,¹ Li Yang,¹ Fei Gao,² and William J. Weber²

¹*Department of Applied Physics, University of Electronic Science and Technology of China, Chengdu 610054, People's Republic of China*

²*Pacific Northwest National Laboratory, P.O. Box 999, Richland, Washington 99352, USA*

(Received 25 January 2007; revised manuscript received 5 April 2007; published 10 July 2007)

Molecular dynamics simulations with Stillinger-Weber potentials were used to study the response of wurtzite-type single-crystalline GaN nanowires to a tensile strain along the axial direction. Nanowires with axial orientations along the [0001], [1 $\bar{1}$ 00], and [11 $\bar{2}$ 0] crystallographic directions, which correspond to experimentally synthesized nanowires, were studied. The results reveal that the nanowires with different axial orientations show distinctly different deformation behaviors under loading. The brittle to ductile transition (BDT) was observed in the nanowires oriented along the [0001] direction and the BDT temperatures lie in the temperature range between 1500 and 1800 K. The nanowires oriented along the [11 $\bar{2}$ 0] direction exhibit slip in the {01 $\bar{1}$ 0} planes, whereas the nanowires oriented along the [1 $\bar{1}$ 00] direction fracture in a cleavage manner under tensile loading. It should be emphasized that multiple yield stresses were observed during different stages in the [11 $\bar{2}$ 0]-oriented nanowires. In general, Young's modulus of the GaN nanowires decreases with decreasing diameter of the nanowires.

DOI: 10.1103/PhysRevB.76.045310

PACS number(s): 62.25.+g, 65.80.+n, 02.70.Ns

I. INTRODUCTION

Wurtzite GaN is a technologically important material for optoelectronics and has a number of potential applications in high-temperature and high-power electronics.^{1,2} Recently, many research groups have studied the synthesis of GaN nanowires (NWs) using various methods, such as laser ablation,³ hydride vapor epitaxy,⁴ and catalytic chemical vapor deposition.⁵⁻¹⁰ Due to its anisotropic and polar nature, GaN exhibits direction-dependent properties,¹¹ and the growth direction of GaN nanowires can be controlled using heteroepitaxy on different single-crystal templates, mediated by catalyst clusters.¹²⁻¹⁶ The most common growth direction for the GaN nanowires is along the [0001] crystalline axes with hexagonal cross sections.¹²⁻¹⁴ Other growth directions along [1 $\bar{1}$ 00] [11 $\bar{2}$ 0] with triangular cross sections have also been synthesized.^{15,16} For example, epitaxial growth of wurtzite gallium nitride on (100) γ -LiAlO₂ and (111) MgO single-crystal substrates results in the selective growth of nanowires in the orthogonal [1 $\bar{1}$ 00] [0001] directions, exhibiting triangular and hexagonal cross sections.¹³ The nanowires grown along different orientations show different properties. Light emission from the [1 $\bar{1}$ 00] wires is blueshifted by \sim 100 meV from that of the [0001] wires.¹³ Recent experiment results^{17,18} have shown that the capacitance of a triangular nanowire is less than that of a cylindrical nanowire of the same size, which could be significant for electronic applications. Such low dimensional GaN-based structures represent important nanometer-scale building blocks for potential optoelectronic, high-temperature and high-power, and spintronic device applications. They are also of fundamental interest in order to understand the role of dimensionality and size in optical, electrical, mechanical, and magnetic properties.

Molecular dynamics (MD) simulations of nanowires have been utilized to provide new insights into nanowire mechani-

cal behavior and deformation mechanisms. A number of studies have used the MD simulations to analyze the tensile failure modes in metal nanowires.¹⁹⁻²⁵ Metal nanowires have been found to exhibit unique physical behavior under tensile loading. Examples of such phenomena are the ability of gold nanowires to form single atom chains under tensile loading,^{21,22} surface stress driven phase transformation of \langle 100 \rangle gold nanowires,^{26,27} shape memory and pseudoelastic behavior of certain face-centered-cubic nanowires,²⁸⁻³⁰ and stress-induced martensitic phase transformation of intermetallic nanowires.³¹ Semiconductor nanowires are also attracting much attention in atomistic simulations because of their successful experimental growth.³²⁻³⁵

In the present study, we performed MD simulations to analyze the deformation of wurtzite-type single-crystalline GaN nanowires with different crystallographic orientations under applied tension. The paper is organized as follows. The details of the MD simulations are described in Sec. II. The results of the numerical simulations concentrating on the different deformation modes observed in the nanowires, which depend on the loading conditions, wire orientations, and temperatures, are presented in Sec. III, along with discussions on the fundamental mechanisms controlling the deformation in the nanowires. Finally, the concluding remarks are summarized in Sec. VI.

II. SIMULATION METHODS

To investigate the atomic structures of single GaN NWs, as observed in experiments,¹²⁻¹⁶ the [0001]-oriented GaN nanowires with hexagonal cross sections and [1 $\bar{1}$ 00]- and [11 $\bar{2}$ 0]-oriented GaN nanowires with triangular cross sections are generated directly from bulk GaN by removing the atoms outside a hexagon or a triangle along the desired axial orientation and replacing them with vacant sites. The top views of these GaN nanowires are shown in Fig. 1. The

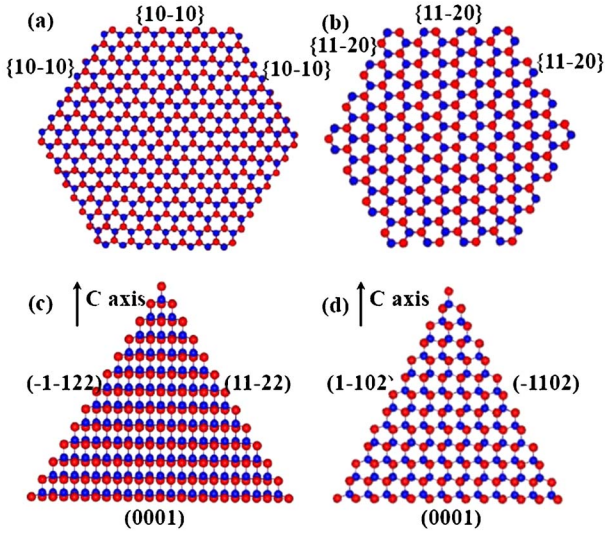


FIG. 1. (Color online) Cross-sectional views of the four types of nanowires used in this work. (a) [0001]-oriented nanowires enclosed with $\{10\bar{1}0\}$ side planes; (b) [0001]-oriented nanowires enclosed with $\{11\bar{2}0\}$ side planes; (c) $[1\bar{1}00]$ -oriented nanowires enclosed with $(11\bar{2}2)$, $(\bar{1}\bar{1}22)$, and (0001) side planes; and (d) $[1\bar{1}00]$ -oriented nanowires enclosed with $(1\bar{1}02)$, $(\bar{1}\bar{1}02)$, and (0001) side planes.

[0001]-oriented nanowires are enclosed with $\{10\bar{1}0\}$ or $\{11\bar{2}0\}$ side planes, while the $[1\bar{1}00]$ -oriented nanowires are enclosed with $(11\bar{2}2)$, $(\bar{1}\bar{1}22)$, and (0001) side planes between which the angles are 63.16° , 58.42° , and 58.42° , respectively. The $[11\bar{2}0]$ -oriented nanowires are enclosed with $(1\bar{1}02)$, $(\bar{1}\bar{1}02)$, and (0001) side planes, as shown in Fig. 1(d). A periodic condition is applied to the axial direction, with a supercell length (L) of 6.12, 6.63, and 6.38 nm for the [0001]-, $[1\bar{1}00]$ -, and $[11\bar{2}0]$ -oriented NWs, respectively. The diameters and numbers of atoms of differently oriented NWs in the present studies are summarized in Table I.

In this work, Stillinger-Weber potentials^{36,37} were used to describe the Ga-Ga, N-N, and Ga-N interatomic interactions in the GaN model nanowires. It has been shown that these potentials reproduce the binding energy, lattice constants, and elastic properties of wurtzite GaN and achieve a realistic description of the microscopic structures and the energetics of different planar defects and their interactions in the wurtzite GaN.³⁷ Although the potentials were calibrated to reproduce bulk structures and mechanical properties, they have been successfully employed to evaluate the Young modulus of defect-free and defected single-crystal GaN nanotubes^{38,39} and to study melting and mechanical behaviors of various GaN nanotubes.^{40,41} In addition, the potentials can handle dangling bonds, wrong bonds, and excess bonds in bulk GaN very well. All of these results have demonstrated that the Stillinger-Weber potentials are capable of describing the equilibrium and deformed structures of crystalline GaN nanowires. It should be noted that the Stillinger-Weber potentials are “short-range potentials,” which include only the first nearest neighbor interactions. This may cause the inter-

TABLE I. The diameters and numbers of atoms of differently oriented NWs used in the present studies.

		Diameter (nm)	No. of atoms
[0001]-oriented NWs with $\{10\bar{1}0\}$ side planes	1	2.02	2304
	2	2.59	3600
	3	3.14	5184
[0001]-oriented NWs with $\{11\bar{2}0\}$ side planes	4	1.92	2016
	5	2.88	4320
	6	3.20	5328
$[1\bar{1}00]$ -oriented NWs	7	2.60	2652
	8	3.12	3756
	9	3.64	5052
$[11\bar{2}0]$ -oriented NWs	10	2.08	1620
	11	2.60	2420
	12	3.12	3380

actions between atoms to abruptly vanish outside a certain radius, and this affects the results somehow. *Ab initio* calculations should provide more accurate results but require extensive computational efforts. However, these short-range potentials should not affect the main conclusions obtained in the present investigations.

A modified version of the MOLDY computer code⁴² was employed in this study, and periodic boundary conditions were applied along the axial direction of the NWs with the *NVT* ensemble (i.e., the number of particles N , the volume V , and the temperature T of the system are kept constant during the simulations). Strain-stress simulations were performed using the procedure that follows. The relative positions of atoms within the three atomic layers at the top and bottom of NWs are fixed during simulations, forming two rigid borders. The initial structures of the NWs were equilibrated for 100 ps at a given temperature, which allows the NWs to have stable configurations. The strain was then applied along the axial direction to study the mechanical properties of the NWs by imposing a displacement of Δz . The atoms in the rigid borders were displaced by $\Delta z/2$, but the coordinates of the remaining atoms were scaled by a factor $(L+\Delta z)/L$ along the z direction. This deformed tube was relaxed for 10 ps, and then the relaxed structure was used as an initial configuration for the next MD simulation.

The following scaling method is adopted to ensure that the temperature of the system remains constant during simulation:⁴³

$$v_i^{new} = v_i \sqrt{\frac{T_D}{T_R}}, \quad (1)$$

where v_i^{new} is the velocity of particle i after correction. T_D and T_R are the desired and actual temperatures of the system, respectively. This scaling method is applied during the simulations for a specific equilibrium temperature.

The localized axial stress for atom i is defined as

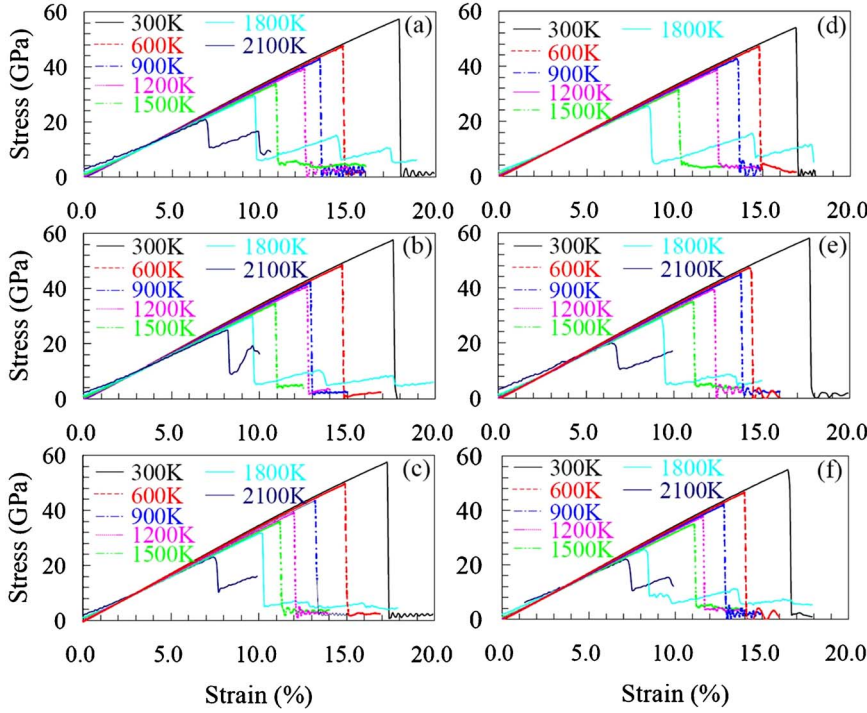


FIG. 2. (Color online) Tensile stress-strain curves for the [0001]-oriented nanowires with a strain rate of 0.001%/ps at various temperatures. The nanowire diameters are (a) 2.02 nm, (b) 2.59 nm, (c) 3.14 nm, (d) 1.92 nm, (e) 2.88 nm, and (f) 3.2 nm, and the length of the nanowires is 6.12 nm. The lateral facets of (a)–(c) and (d)–(f) are $[10\bar{1}0]$ and $[11\bar{2}0]$, respectively.

$$\eta_z^i(\varepsilon_z) = \frac{1}{V_i} \left[m_i v_z^i v_z^i + \frac{1}{2} \sum_{j=1}^N F_z^{ij}(\varepsilon_z) r_z^{ij}(\varepsilon_z) \right], \quad (2)$$

where m_i is the mass of atom i , v_z^i is the velocity along the axis direction, and F_z^{ij} refers to the component of the interatomic force along the axis direction between atoms i and j . r_z^{ij} is the interatomic distance along the axis direction between atoms i and j . V_i refers to the volume of atom i , which was assumed as a hard sphere in a closely packed crystal structure. The axial stress of a nanowire is taken as the arithmetic mean of the local stresses over all the atoms given by

$$\sigma_z = \frac{1}{N} \sum_{i=1}^N \eta_z^i. \quad (3)$$

The normal strain along the axial direction, ε_z , is calculated as

$$\varepsilon_z = \frac{\overline{l_{z(t)}} - l_{z(0)}}{l_{z(0)}}, \quad (4)$$

where $\overline{l_{z(t)}}$ is the average length along the axial direction at time t and $l_{z(0)}$ is the initial average length of the nanowire. The strain rate is calculated as

$$\dot{\varepsilon} = \frac{\varepsilon_z}{s\Delta t}, \quad (5)$$

where s is the number of relaxation steps after each strain increment and Δt is the simulation time step. In the present study, the simulation time step was fixed to be 0.5 fs (0.5×10^{-15} s) and the number of relaxation steps was fixed to be 20 000 steps. However, the strain increment was varied, using $\varepsilon_z = 0.001$, 0.000 75, and 0.0005, i.e., simulating strain

rates of 0.01%, 0.0075%, and were used in this work. The stress during each strain increment was computed by averaging over the final 2000 relaxation steps, and the corresponding stress-strain relationship of the GaN NWs can be obtained by using Eqs. (3) and (4)

III. RESULTS AND DISCUSSIONS

A. Tension of [0001]-oriented nanowires

The melting temperatures of [0001]-oriented nanowires have been studied, and the results show that the melting temperatures increase to saturation values of about 3100 and 2900 K when the diameters of the nanowires are larger than 3.14 and 4.14 nm for the nanowires with $[10\bar{1}0]$ - and $[10\bar{2}0]$ -oriented lateral facets, respectively.⁴⁴ The mechanical behavior of these nanowires is studied between the temperatures of 300 and 2100 K, which are lower than the melting temperatures. The relationships between tensile stress and strain for the [0001]-oriented nanowires are shown in Fig. 2 with a strain rate of $0.01\% \text{ ps}^{-1}$ at various temperatures. All the nanowires considered here correspond to the applied strain in the same way but with the different nanowire diameters. For low strains, the stress-strain relationship follows Hooke's law, and the stress increases almost linearly with increasing strain up to a threshold value that is defined as the critical stress. It is of interest to note that the stress-strain curves show different behaviors at low and high temperatures when the strain is larger than the critical strain. At temperatures below 1500 K, further increases in strain lead to abrupt decreases in stress, whereas the stress-strain curves show zigzag behavior after the critical strain at higher temperatures. For example, in the [0001]-oriented nanowires with a diameter of 2.02 nm, the stress increases with increas-

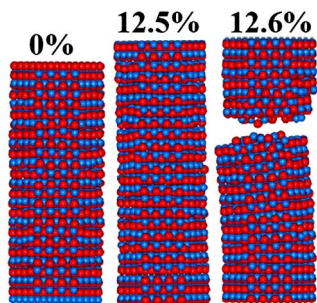


FIG. 3. (Color online) Atomic configurations of selected stages for the $[0001]$ -oriented nanowire with $[10\bar{1}0]$ -oriented lateral facets and a diameter of 2.02 nm at the temperature of 1200 K.

ing strain up to 57.18 GPa (at strain of 17.9%), and further increases in strain lead to abrupt decreasing of stress to ~ 0.0 GPa at 300 K. These results demonstrate that the nanowires fail in a brittle manner at low temperatures. However, the stress-strain relation displays a zigzag behavior after a critical stress level of 29.25 GPa (at strain of 9.7%) at 1800 K, and multiple maximums appear along the path. These multiple maximum stresses suggest that the nanowires have the multiple yield stresses before they completely fail. It was observed that the stress required to produce the second decrease was much smaller than that required to produce the initial decrease. From Fig. 2, it can be noted that the critical stress at low temperatures is larger than that at higher temperatures. As the temperature increases, a large number of atoms gain sufficient energy to overcome the activation energy barrier, and hence plastic deformation occurs, which may suggest that a thermally activated process plays a predominant role in the elongation of GaN NWs.

Figures 3–5 show the side views of the atomic configurations at several stages of stretching the $[0001]$ -oriented nanowire with $[10\bar{1}0]$ -oriented lateral facets and a diameter of 2.02 nm at the simulation temperatures of 1200, 1500, and 1800 K, respectively, where the strain rate is 0.01%/ps. At 1200 K and up to strain of 12.5%, the Ga–N bond lengths increase uniformly and no structural defects appear in the nanowires. Upon passing the critical strain, the Ga–N bond experiences an abrupt rupture, and the nanowires fail with a clean cut, without any observed necking. The abrupt rupture of the bond leads to abrupt dropping of stress. At 1500 K, the nanowires are highly ordered and retain a stretched hexagonal structure until the first discontinuity in the tensile stress

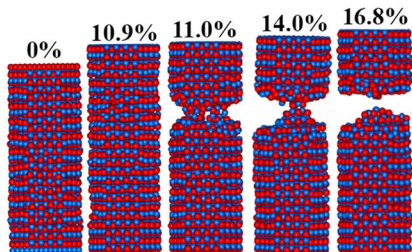


FIG. 4. (Color online) Atomic configurations of selected stages for the $[0001]$ -oriented nanowire with $[10\bar{1}0]$ -oriented lateral facets and a diameter of 2.02 nm at 1500 K.

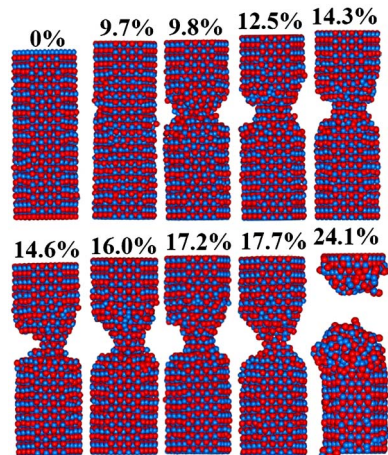


FIG. 5. (Color online) Atomic configurations of selected stages for the $[0001]$ -oriented nanowire with $[10\bar{1}0]$ -oriented lateral facets and a diameter of 2.02 nm at the simulation temperature of 1800 K.

that appears at the strain of 11.0%. The nanowires rupture at the strain of 16.8%. At 1800 K, the extension of the nanowire starts with an elastic deformation from its initial state to a strain of 9.7%. Upon reaching the critical strain, the nanowire experiences an abrupt bond rupture, which subsequently results in surface rupture. After this, the nanowire recrystallizes to a new but dislocated configuration, and further increase in strain up to 14.3% leads to the emission of a second dislocation. The above process is repeated until the nanowire ruptures. During the entire deformation process, necking of the nanowires is observed. The surface rupture of the nanowire leads to the multiple yield stresses along the path, as observed in Fig. 2, which results in the failing of the nanowire in a ductile manner.

Figure 6 shows the atomic configurations in selected stages for the $[0001]$ -oriented nanowires with $[11\bar{2}0]$ -oriented lateral facets and with the diameter of 2.88 nm at the simulation temperatures of 600, 1200, and 1800 K. These configurations also confirm that the nanowires rupture in a brittle manner at low temperatures and in a ductile manner at high temperatures. It is also noted that some atoms become free from the wire surfaces, and this may be due to the short-range potentials employed, as discussed in the Sec. II.

From the above results, it can be concluded that the mechanical properties of $[0001]$ -oriented nanowires are sensitive to temperature, and the nanowires exhibit ductility at high deformation temperatures and brittleness at lower temperatures. The brittle to ductile transition (BDT) can be determined, and it lies in the temperature range between 1500 and 1800 K. At higher temperatures, the atomic structure has higher entropy, and its constituent atoms vibrate about their equilibrium positions at much larger amplitude, as compared to atomic vibrational modes at lower temperatures, and hence plastic deformation occurs at higher temperatures.

B. Strain effect on the tension of $[0001]$ -oriented nanowires

Since the nanowire failure occurs as a result of dynamic processes, the mechanisms of material deformation can also

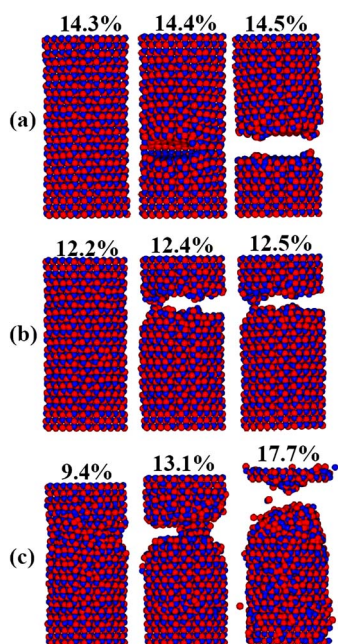


FIG. 6. (Color online) Atomic configurations of selected stages for the [0001]-oriented nanowires with [1120]-oriented lateral facets and a diameter of 2.88 nm at the simulation temperatures of (a) 600 K, (b) 1200 K, and (c) 1800 K.

be influenced by strain rate. Therefore, the effect of strain rate on the tensile behavior is also investigated for the [0001]-oriented nanowires, but only for those with [1120]-oriented lateral facets. Figure 7 presents the stress-strain curves of [0001]-oriented nanowires with a diameter of 1.92 nm with the strain rates of 0.0005%/ps, 0.00075%/ps, and 0.001%/ps at a simulation temperature of 1500 K. For all the strain rates applied, the stresses increase linearly with strain up to 10.1%. Below this limit, the stress-strain curves for the three strain rates almost completely overlap. This implies that the strain rate has no significant effect on the elastic properties of GaN nanowires. An abrupt decrease of the stress can be clearly seen at the critical strain for the strain rates of 0.00075%/ps and 0.001%/ps, whereas the stress-strain curve for the strain rate of 0.0005%/ps exhibits a zigzag behavior. For the strain rate of 0.001%/ps, the critical

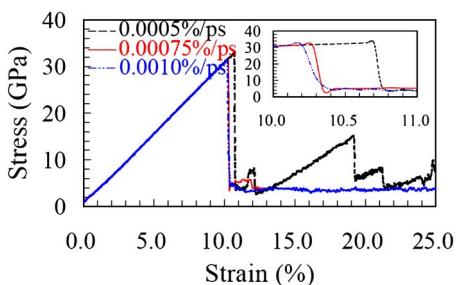


FIG. 7. (Color online) Tensile stress-strain curves for the [0001]-oriented nanowires with [1120]-oriented lateral facets and a diameter of 1.92 nm, with strain rates of 0.0005%/ps, 0.00075%/ps, and 0.001%/ps at 1500 K. The inset shows the enlarged parts of strains between 10% and 11%.

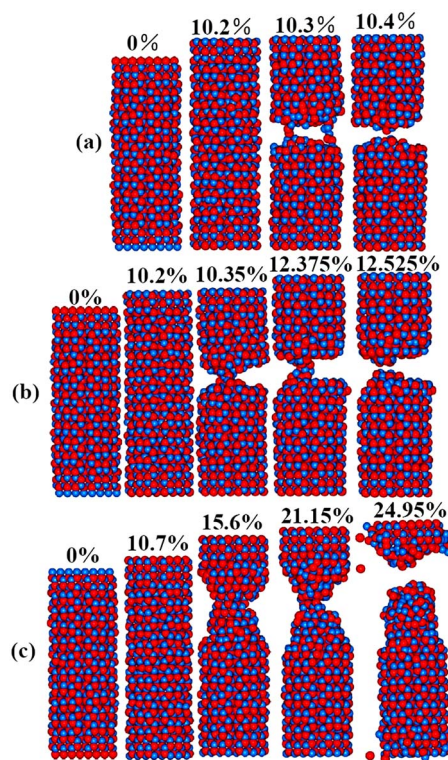


FIG. 8. (Color online) Atomic configurations of selected stages for the [0001]-oriented nanowires with [1120]-oriented lateral facets and a diameter of 1.92 nm with strain rates of (a) 0.001%/ps, (b) 0.00075%/ps, and (c) 0.0005%/ps at the simulation temperature of 1500 K.

stress is 31.43 GPa at the strain of 10.2%, while for the strain rates of 0.00075%/ps and 0.0005%/ps, the critical stresses are 31.25 and 33.02 GPa at the strains of 10.275% and 10.7%, respectively. Obviously, the lower strain rates result in larger critical strains. The atomic configurations during selected stages upon stretching of the nanowires, as shown in Fig. 8, reveal that the nanowire ruptures in a brittle manner at the strain rates of 0.00075%/ps and 0.001%/ps but in a ductile manner at the strain rate of 0.0005%/ps. The results indicate that the BDT temperatures shift to lower temperatures with decrease in strain rate. This may be explained by the fact that, due to the high strain rate, the material does not have enough time to rearrange the configuration of the atom system, and hence the bond ruptures abruptly, whereas with a low strain rate, the atoms have enough time to relax and rearrange their configurations, which leads to plastic deformation.

The above results show that the yield behavior of the [0001]-oriented GaN nanowires depends on temperature, i.e., yield by cleaving at lower temperatures and by necking at high temperatures. In order to investigate the origins of the difference in the ductile and brittle behaviors of the nanowires, the evolution of atomic configurations is carefully examined. The evolution of atomic configurations suggests a brittle response [Figs. 3, 6(a), 6(b), and 8(a)], consisting of cleavage fracture along (0001) planes at lower temperatures. The different atomic configurations of the cross section of the neck at different stages, along with the stress-strain curve

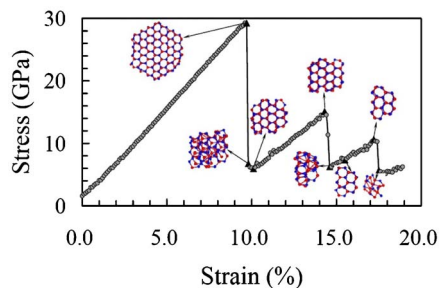


FIG. 9. (Color online) Atomic configurations of the cross section within the neck, along with the stress-strain curve for the [0001]-oriented nanowire with a diameter of 2.02 nm at the simulation temperature of 1800 K.

for the [0001]-oriented nanowire with a diameter of 2.02 nm at the simulation temperature of 1800 K, are shown in Fig. 9. As seen from the figure, the cross section shows little change as the strain increased from 0% to 9.7%, but the bonds of the surface atoms rupture and the atoms within the neck almost randomize with increasing strain up to 9.8%, forming an amorphouslike structure. Then, the atoms relax and recover to their normal crystal positions, and the atomic configurations reach another stable configuration. The bond rupture of the surface atoms and relaxation of other atoms induce the drop of the stress. The stress increases with the further increasing of strain to 14.3%, but little change of the cross section is observed. Then, rupture of the bonds of the surface atoms and the randomization of the central atoms within the neck occur again at strain of 14.6%, which induces the second drop of the stress. The above procedure repeats until the nanowire ruptures completely. The results indicate that plastic deformation takes place through a phase transformation from crystal to amorphous structure and generally starts from the surface of GaN nanowires at higher temperatures.

C. Tension of $[1\bar{1}00]$ -oriented nanowires

Figure 10 shows the stress-strain curves for the $[1\bar{1}00]$ -oriented nanowires subject to uniaxial tensile loading with a strain rate of $0.01\% \text{ ps}^{-1}$ at various temperatures. The nanowires deform elastically until a critical strain is reached, and the nanowires yield, after which bond breaking occurred and a significant decrease in stress appears. For the nanowires with a diameter of 2.60 nm, the stress increases with increasing strain up to 36.52 GPa (at strain of 15.7%), but the further increase in strain leads to abrupt decreasing of stress to 0.0 GPa at 500 K. The side views of the atomic configurations at several stages of stretching these nanowires at the simulation temperature of 500 K are shown in Fig. 11. It can be seen that the Ga–N bond lengths initially increase uniformly and no structural defects appear in the NWs. Upon reaching a critical strain of 15.7%, the crystal structure experiences an abrupt bond rupture, and then the nanowire ruptures with a clean cut, without any observed necking. Figure 12 shows the side views of the atomic configurations of the ruptured nanowire with a diameter of 3.64 nm at 300, 900, and 1500 K. The nanowire ruptures with a clean cut at all the

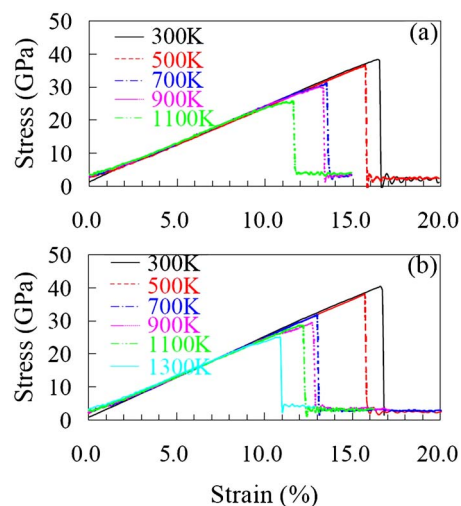


FIG. 10. (Color online) Tensile stress-strain curves for the $[1\bar{1}00]$ -oriented nanowires subject to uniaxial tensile loading with a strain rate of $0.01\% \text{ ps}^{-1}$ at various temperatures with the diameters of (a) 2.60 nm and (b) 3.12 nm.

simulation temperatures considered, which suggests that the $[1\bar{1}00]$ -oriented nanowires rupture in a brittle manner.

D. Tension of $[11\bar{2}0]$ -oriented nanowires

In this section, we present numerical simulations of the $[11\bar{2}0]$ -oriented nanowires. Stress-strain curves during the deformation process are given in Fig. 13, whereas the side views of the atomic configurations at several stages for a nanowire with a diameter of 2.08 nm at 500 K are shown in Fig. 14. All the nanowires show a linear stress-strain response for all applied strains up to a critical value, but a sudden decrease in stress is observed at first yield. At this point, the nanowire slips in a $\{01\bar{1}0\}$ plane, which leads to the stress relaxation, and a portion of the crystal structure is

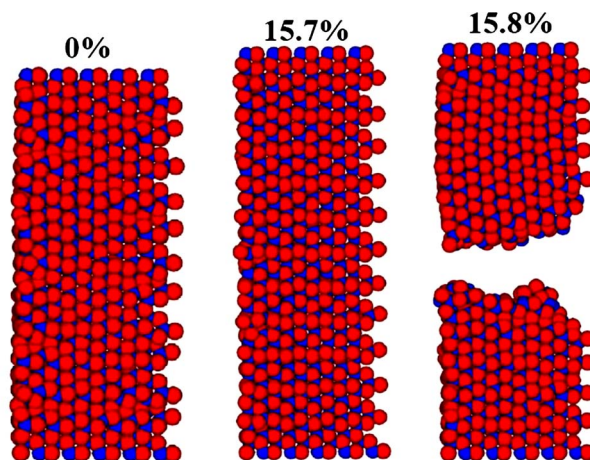


FIG. 11. (Color online) Side views of the atomic configurations at several stages of stretching the $[1\bar{1}00]$ -oriented nanowire with a diameter of 2.60 nm at 500 K.

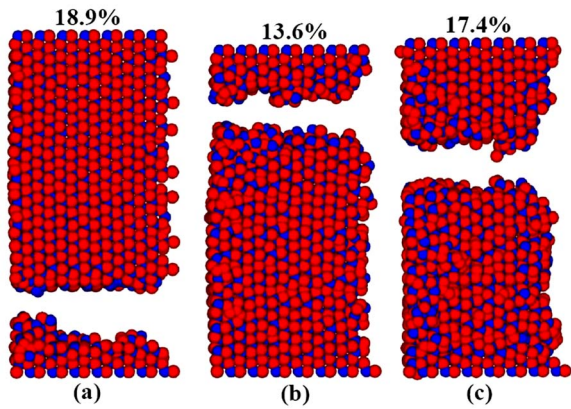


FIG. 12. (Color online) Side views of the atomic configurations of ruptured $[1\bar{1}00]$ -oriented nanowires with a diameter of 3.64 nm at (a) 300 K, (b) 900 K, and (c) 1500 K.

displaced. Upon full relaxation, the nanowire undergoes a second cycle of linear stress-strain increment, until a new slip is developed. This causes the whole cycle to repeat itself. The cyclical stress-strain progression of such plastic deformation significantly weakens the nanowire structure, and thereby causes a progressively lower yield stress at each subsequent cycle. However, the present results have demonstrated that the $[11\bar{2}0]$ -oriented nanowires have the multiple yield stresses along their strain path for all the temperatures considered. The side views of the several atomic configurations of the nanowire with a diameter of 2.60 nm at 500 K are shown in Fig. 15(a) and those with a diameter of 3.12 nm at 500 and 1300 K are presented in Figs. 15(b) and 15(c), respectively. These atomic configurations confirm that the slip occurred in the $\{01\bar{1}0\}$ planes. Interestingly, the strain-stress behavior of the $[11\bar{2}0]$ -oriented nanowires is different from that observed in the $[0001]$ - and $[1\bar{1}00]$ -oriented nanowires that rupture in a brittle or a ductile manner.

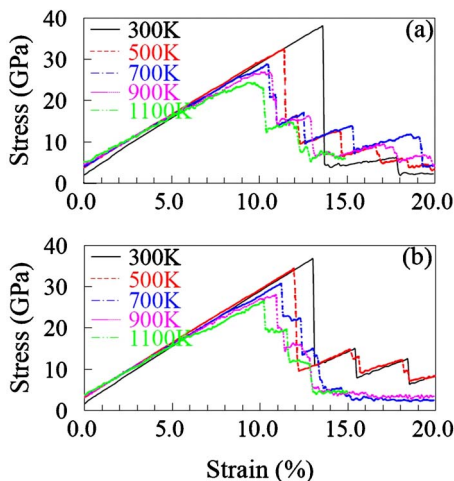


FIG. 13. (Color online) Tensile stress-strain curves for the $[11\bar{2}0]$ -oriented nanowires subject to uniaxial tensile loading with a strain rate of $0.01\% \text{ ps}^{-1}$ at various temperatures with the diameters of (a) 2.08 nm and (b) 2.60 nm.

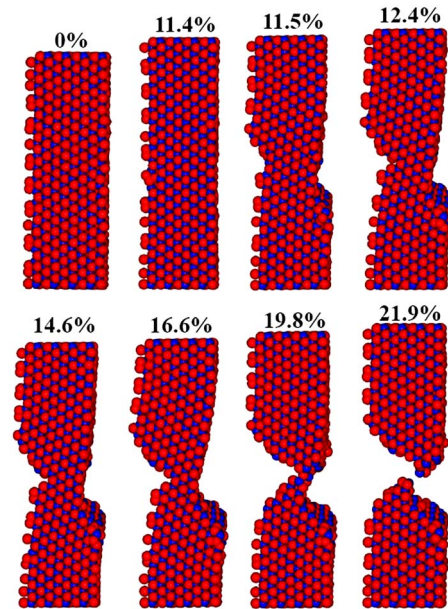


FIG. 14. (Color online) Side views of the atomic configurations at several stages of stretching the $[11\bar{2}0]$ -oriented nanowires with a diameter of 2.08 nm at the simulation temperature of 500 K.

The mechanical behavior shows difference in behaviors for the three types of oriented nanowires. The brittle to ductile transition can be observed in the nanowires oriented along the $[0001]$ direction. The nanowires oriented along the $[11\bar{2}0]$ direction exhibit slip in the $\{01\bar{1}0\}$ planes, whereas the nanowires oriented along the $[1\bar{1}00]$ direction fracture in a cleavage manner under tensile loading. The difference can be clarified by the bond configuration in wurtzite GaN, as shown in Fig. 16. As the strain is applied along the $[0001]$ direction, all the bonds can be stretched. The origin of the brittle to ductile transition has been discussed in Sec. III. As the strain is applied along the $[11\bar{2}0]$, only the N1-Ga4, N2-Ga4, N3-Ga4, N4-Ga1, N4-Ga2, and N4-Ga3 bonds can be stretched. The force on N1-Ga4 bond generated by the strain will be larger than that on the N2-Ga4 and N3-

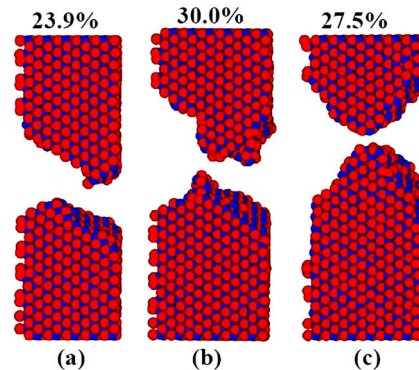


FIG. 15. (Color online) Side views of the atomic configurations of a ruptured nanowire with a diameter of 2.60 nm at the simulation temperature of (a) 500 K and the nanowires with a diameter of 3.12 nm at the simulation temperatures of (b) 500 K and (c) 1300 K.

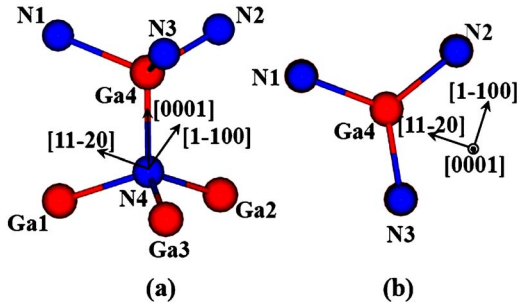


FIG. 16. (Color online) (a) Side view and (b) top view of bond configurations of wurtzite GaN.

Ga4 bonds, so N1–Ga4 ruptures easily, which induces the slip in the N2–Ga4–N3 plane, i.e., the $\{01\bar{1}0\}$ planes. As the strain is applied along the $[1\bar{1}00]$ direction, only the N2–Ga4, N3–Ga4, N4–Ga2, and N4–Ga3 bonds can be stretched, and the forces on N2–Ga4 and N3–Ga4 bonds are equal, which induces the cleavage fracture along $\{1\bar{1}00\}$ planes.

E. Young's modulus of the nanowires

There are two approaches to obtain Young's modulus, i.e., force approach and energy approach.⁴⁵ For the force approach, Young's modulus can be directly obtained from the ratio of stress to strain, whereas the energy approach calculates Young's modulus from the second derivative of strain energy with respect to the strain per unit volume. In the present study, the force approach is adopted to evaluate Young's modulus of the nanowires. Young's modulus can be determined from the results of the tension tests for the strain $<2.5\%$ using liner regression and the calculated results for all the nanowires are shown in Fig. 17. Young's modulus of the $[0001]$ -oriented nanowires is between 347 and 249 GPa at the temperatures between 300 and 2100 K, while it is in the ranges of 254–179, and 284–228 GPa for the $[1\bar{1}00]$ - and $[11\bar{2}0]$ -oriented nanowires, respectively, at the tempera-

tures ranging between 300 and 1100 K. The calculated values generally agree well with the experimental results of 227–305 GPa of GaN nanowires.⁴⁶ It is shown that Young's modulus decreases with increasing temperature, which suggests that the nanowires become softened at higher temperatures because of higher kinetic energy of each atom in average, which will result in easier slipping and elongation of the nanowires. From Fig. 17, it can also be seen that Young's modulus decreases with decreasing the diameter of the nanowires which is somewhat unexpected, in contrast to the single-crystal materials, where Young's modulus is expected to increase with decreasing crystal size.^{47,48} However, the results agree well with recent experimental result.⁴⁶ The reason for this behavior may be the small atomic-coordination number and weak cohesion of the atoms near the surface, as compared with those in the bulk, and the increasing dominance of the surface would decrease the rigidity of the structure.⁴⁹

IV. SUMMARY AND CONCLUSIONS

In conclusion, we have studied the fundamental deformation mechanism in GaN nanowires with different orientations under tension using MD simulations. Several interesting features relating to its crystal orientation were observed. Due to its high crystal stability at low temperatures, the deformation behavior of the $[0001]$ -oriented nanowires was characterized by brittle rupture. At higher temperatures, the crystal structure became less stable due to higher amplitude of atomic vibration around their equilibrium positions. The deformation of the nanowires changes from a brittle rupture to a ductile rupture with increasing temperature. The BDT was observed in the $[0001]$ -oriented nanowires and the corresponding temperatures lie in the range between 1500 and 1800 K. The mechanisms of material deformation can also be influenced by strain rate. The nanowires rupture in a brittle manner at high strain rate and in a ductile manner at low strain rate. Interestingly, the $[11\bar{2}0]$ -oriented nanowires slip in the $\{01\bar{1}0\}$ planes and there exist multiple yield

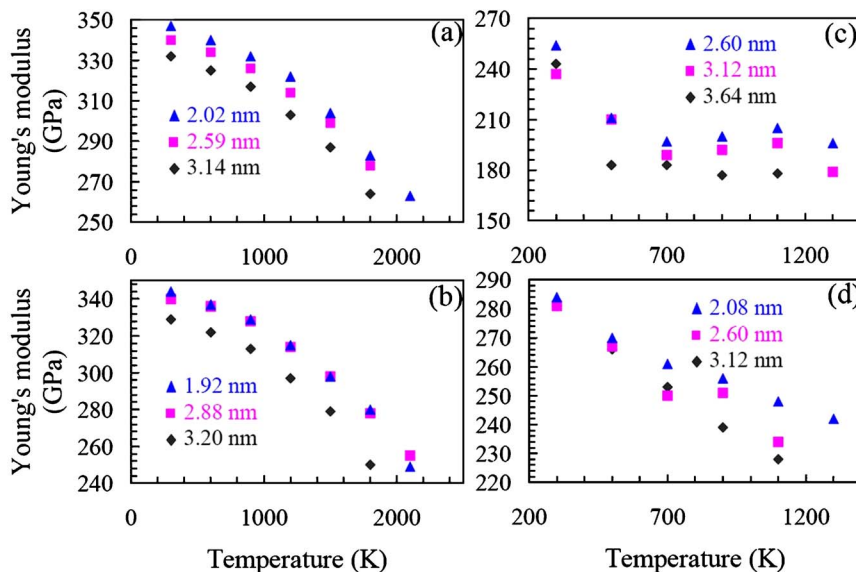


FIG. 17. (Color online) Young's modulus of (a) the $[0001]$ -oriented nanowires with $\{01\bar{1}0\}$ side planes, (b) the $[0001]$ -oriented nanowires with $\{11\bar{2}0\}$ side planes, and (c) the $[1\bar{1}00]$ - and (d) $[11\bar{2}0]$ -oriented nanowires at various simulation temperatures.

stresses along the strain path, whereas the $[1\bar{1}00]$ -oriented nanowires fracture in a cleavage manner under tensile loading. Finally, it was found that Young's modulus of the GaN nanowires decreases with decreasing diameter of the nanowires, which agrees well with recent experimental results.

ACKNOWLEDGMENTS

Z.W. is grateful for the support from the Overseas' Scholarship Program of the University of Electronic Science and

Technology of China during a visiting scholar assignment at the Pacific Northwest National Laboratory. Z.W. and X.Z. are grateful for the Program for Innovative Research team in UESTC. F.G. and W.J.W. were supported by the Division of Materials Sciences and Engineering, Office of Basic Energy Sciences, U.S. Department of Energy under Contract No. DE-AC05-76RL01830. The authors also wish to thank the Molecular Science Computing Facility in the Environmental Molecular Sciences Laboratory at the Pacific Northwest National Laboratory for a grant of computer time.

*Corresponding author; zgwang_dr@yahoo.com

- ¹J. C. Johnson, H. J. Choi, K. P. Knutsen, R. D. Schaller, P. D. Yang, and R. J. Saykally, *Nat. Mater.* **1**, 106 (2002).
- ²H. Morkoc, S. Strite, G. B. Gao, M. E. Lin, B. Sverdlov, and M. Burns, *J. Appl. Phys.* **76**, 1363 (1994).
- ³X. F. Duan and C. M. Lieber, *J. Am. Chem. Soc.* **122**, 188 (2000).
- ⁴G. Seryogin, I. Shalish, W. Moberlychan, and V. Narayanamurti, *Nanotechnology* **16**, 2342 (2005).
- ⁵E. Stern *et al.*, *Nanotechnology* **16**, 2941 (2005).
- ⁶T. Wang, F. Ranalli, P. H. Parbrook, R. Airey, J. Bai, R. Rattlidge, and G. Hill, *Appl. Phys. Lett.* **86**, 103103 (2005).
- ⁷D. S. Han, J. Park, K. W. Rhie, S. Kim, and J. Chang, *Appl. Phys. Lett.* **86**, 032506 (2005).
- ⁸S. K. Lee, H. J. Choi, P. Pauzauskie, P. D. Yang, N. K. Cho, H. D. Park, E. K. Suj, K. Y. Lim, and H. J. Lee, *Phys. Status Solidi B* **241**, 2775 (2004).
- ⁹X. H. Chen, J. Xu, R. M. Wang, and D. P. Yu, *Adv. Mater. (Weinheim, Ger.)* **15**, 419 (2003).
- ¹⁰G. Kipshidze, B. Yavich, A. Chandolu, J. Yun, V. Kuryatkov, I. Ahmad, D. Aurongzeb, M. Holtz, and H. Temkin, *Appl. Phys. Lett.* **86**, 033104 (2005).
- ¹¹P. Waltereit, O. Brandt, A. Trampert, H. T. Grahn, J. Menniger, M. Ramsteiner, M. Reiche, and K. H. Ploog, *Nature (London)* **406**, 865 (2000).
- ¹²B. D. Liu, Y. Bando, C. C. Tang, F. F. Xu, and D. Golberg, *Appl. Phys. Lett.* **87**, 073106 (2005).
- ¹³T. Kuykendall, P. J. Pauzauskie, Y. F. Zhang, J. Goldberger, D. Sirbulu, J. Denlinger, and P. D. Yang, *Nat. Mater.* **3**, 524 (2004).
- ¹⁴J. Zhang, L. D. Zhang, X. F. Wang, C. H. Liang, X. S. Peng, and Y. W. Wang, *J. Chem. Phys.* **115**, 5714 (2001).
- ¹⁵S. Y. Bae, H. W. Seo, J. Park, H. Yang, H. Kim, and S. Kim, *Appl. Phys. Lett.* **82**, 4564 (2003).
- ¹⁶T. Kuykendall, P. Pauzauskie, S. Lee, Y. F. Zhang, J. Goldberger, and P. D. Yang, *Nano Lett.* **3**, 1063 (2003).
- ¹⁷D. Vashaee, A. Shakouri, J. Goldberger, T. Kuykendall, P. Pauzauskie, and P. Yang, *J. Appl. Phys.* **99**, 054310 (2006).
- ¹⁸S. Gradečak, F. Qian, Y. Li, H. G. Park, and C. M. Lieber, *Appl. Phys. Lett.* **87**, 173111 (2005).
- ¹⁹S. J. A. Koh, H. P. Lee, C. Lu, and Q. H. Cheng, *Phys. Rev. B* **72**, 085414 (2005).
- ²⁰H. S. Park and J. A. Zimmerman, *Phys. Rev. B* **72**, 054106 (2005).
- ²¹E. Z. da Silva, A. J. R. da Silva, and A. Fazzio, *Phys. Rev. Lett.* **87**, 256102 (2001).
- ²²E. Z. da Silva, F. D. Novaes, A. J. R. da Silva, and A. Fazzio, *Phys. Rev. B* **69**, 115411 (2004).
- ²³H. S. Park and J. A. Zimmerman, *Scr. Mater.* **54**, 1127 (2006).
- ²⁴H. S. Park, K. Gall, and J. A. Zimmerman, *J. Mech. Phys. Solids* **54**, 1862 (2006).
- ²⁵S. J. A. Koh and H. P. Lee, *Nanotechnology* **17**, 3451 (2006).
- ²⁶J. Diao, K. Gall, and M. L. Dunn, *Nat. Mater.* **2**, 656 (2003).
- ²⁷K. Gall, J. Diao, M. L. Dunn, M. Haftel, N. Bernstein, and M. J. Mehl, *J. Eng. Mater. Technol.* **127**, 417 (2005).
- ²⁸H. S. Park, K. Gall, and J. A. Zimmerman, *Phys. Rev. Lett.* **95**, 255504 (2005).
- ²⁹W. W. Liang and M. Zhou, *Phys. Rev. B* **73**, 115409 (2006).
- ³⁰W. W. Liang and M. Zhou, *Nano Lett.* **5**, 2039 (2005).
- ³¹H. S. Park, *Nano Lett.* **6**, 958 (2006).
- ³²M. A. Makeev, D. Srivastava, and M. Menon, *Phys. Rev. B* **74**, 165303 (2006).
- ³³T. Y. Kim, S. S. Han, and H. M. Lee, *Mater. Trans.* **45**, 1442 (2004).
- ³⁴A. J. Kulkarni, M. Zhou, K. Sarasamak, and S. Limpijumnong, *Phys. Rev. Lett.* **97**, 105502 (2006).
- ³⁵A. J. Kulkarni, M. Zhou, and F. J. Ke, *Nanotechnology* **16**, 2749 (2005).
- ³⁶F. H. Stillinger and T. A. Weber, *Phys. Rev. B* **31**, 5262 (1985).
- ³⁷J. Kioseoglou, H. M. Polatoglou, L. Lymperakis, G. Nouet, and Ph. Komninou, *Comput. Mater. Sci.* **27**, 43 (2003).
- ³⁸B. Xu, A. J. Lu, B. C. Pan, and Q. X. Yu, *Phys. Rev. B* **71**, 125434 (2005).
- ³⁹B. Xu and B. C. Pan, *J. Appl. Phys.* **99**, 104314 (2006).
- ⁴⁰Z. G. Wang, X. T. Zu, F. Gao, and W. J. Weber, *J. Appl. Phys.* **100**, 063503 (2006).
- ⁴¹Z. G. Wang, X. T. Zu, F. Gao, and W. J. Weber, *Appl. Phys. Lett.* **89**, 243123 (2006).
- ⁴²F. Gao, E. J. Bylaska, and W. J. Weber, *Phys. Rev. B* **70**, 245208 (2004).
- ⁴³J. M. Haile, *Molecular Dynamics Simulation* (Wiley, New York, 1992).
- ⁴⁴Z. G. Wang, X. T. Zu, F. Gao, and W. J. Weber, *J. Mater. Res.* **22**, 742 (2007).
- ⁴⁵H. Raffi-Tabar, *Phys. Rep.* **390**, 235 (2004).
- ⁴⁶C. Y. Nam, P. Jaroenapibal, D. Tham, D. E. Luzzi, S. Evoy, and J. E. Fisher, *Nano Lett.* **6**, 153 (2006).
- ⁴⁷A. J. Kulkarni, M. Zhou, and F. J. Ke, *Nanotechnology* **16**, 2749 (2005).
- ⁴⁸C. Q. Chen, Y. Shi, Y. S. Zhang, J. Zhu, and Y. J. Yan, *Phys. Rev. Lett.* **96**, 075505 (2006).
- ⁴⁹M. Schmid, W. Hofer, P. Varga, P. Stoltze, K. W. Jacobsen, and J. K. Nørskov, *Phys. Rev. B* **51**, 10937 (1995).